Seismic Performance of Reinforced And Unreinforced Masonry Brick Walls Assembled With Head-Straight Texture Order)

Toshikazu Ikemoto(1), Reza Amiraslanzadeh(2), Saiji Fukada(3) , Masakatsu Miyajima(4) and Abdolhossein Fallahii(5)

(1) Associate professor, Faculty of Environmental Design, Kanazawa University, tikemoto@se.kanazawa-u.ac.jp
(2) insulator, Faculty of Engineering, Islamic Azad University, reza.amiraslanzadeh@gmail.com
(3) Associate professor, Faculty of Environmental Design, Kanazawa University, saiji@se.kanazawa-u.ac.jp
(4) Professor, Faculty of Environmental Design, Kanazawa University, miyajima@se.kanazawa-u.ac.jp
(3) Assistant professor, Faculty of Engineering, Azerbaijan Shahid Madani Universit, fallahi@azaruniv.edu

Abstract

As we know there are different types of texture order for brick arrangement in construction of brick walls. Among these methods, the one which is very customary, known as head-straight texture order. In process of construction using this technique because of special arrangement of masonry units, some regular interval voids appear over the height of the wall. In this study through filling the holes using steel fiber concrete, we tried to study the roles of these regular slim concrete columns on seismic performance and failure modes of masonry walls. For this purpose four specimens with different level of pre-compression vertical load, have been designed and cyclic loading test were carried out according to evaluate in-plane shear behavior and identification of shear strength, ductility and stiffness degradation of aforementioned panels. Four specimens are two panels without concrete cores and two panels with fiber concrete cores. The results showed that all the specimens failed due to development of horizontal cracks from sides to the middle in the first layer from the bottom of the specimen. Comparisons were made along the results of seismic analysis of two types of masonry panels. The results evidence that existing of fiber concrete columns despite having positive effect on the shear resistance of the walls, causes significant influence of the seismic performance such as ductility.

Keywords: Masonry brick walls, fiber concrete cores, Seismic performance

1. Introduction

Unreinforced masonry building (URM) due to its mechanical properties, durability and thermal isolation is one of the most useful and famous type of construction in the world [1]. Despite this method of building demonstrates acceptable compression strength, it can scarcely bear shear and tensile stress. In most parts of the world URM structures have been located on seismically active regions [2]. As we know earthquakes impose lateral forces to the structures which produce shear and tension stress among the structural components that makes this kind of construction more vulnerable. Hence as available in the literature, in the recent decades researchers have been concerned toward both numerical [3-5] and empirical studying of URM constructions [6,7]. Despite empirical researches are almost costly, time consuming and more onerous, the results are more confident and reliable. Nevertheless, because of complexity and crucial influence of masonry type on the behavior of this kind of structure it is essential and vital to perform more studies and investigations in this regard.

As mentioned in case of lateral loads shear strength plays crucial role on the performance of masonry structures. This parameter severely affected by properties of the constituent materials and geometric texture of masonry units. There are several types of texture order for brick arrangement in the world due to different models of masonry constructions and expected wall thickness (See **Fig. 1**). As we know for load bearing walls the thickness of masonry is typically larger than the length of the unit. On the other word two masonry units is used on the width of the wall leading to some unique types of brick order. More studies have been implemented in recent decades in order to evaluate and characterize seismic behavior and performance of this structural element [8,9]. But a few of these empirical programs was considered thickness of the wall and texture order corresponded to a load bearing walls width. Among the most famous texture types, the one which is very customary in Middle East countries, known as Head-straight order. This texture type is known as double Flemish bond in western countries. Using this order thickness of the wall, varies between 30 to 40 cm depended on the unit length. For construction of brick walls using mentioned technique, each header is centered on the stretcher above and below. In other words, bond, consisting of alternate headers and stretchers in each course is constructed. In front side at first brick by length of three-quarters is placed straight along the wall stretches. Then next unit is placed perpendicular to the head joint of the first unit. This procedure continues along the wall stretches using full size brick units and will again end to a three-quarters straight brick unit. Back side of the wall has a simple head-straight order but using full size bricks. The order of front and back side of the wall in next layer has the inverse order of first layer (**Fig. 2**).

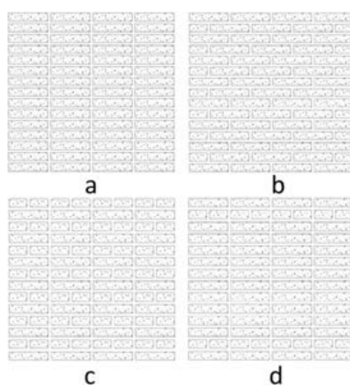

Fig. 1-Various types of texture orders for brick masonry: (a) stack bond, (b) stretcher bond, (c) English (or cross) bond, (d) American (or common) bond.

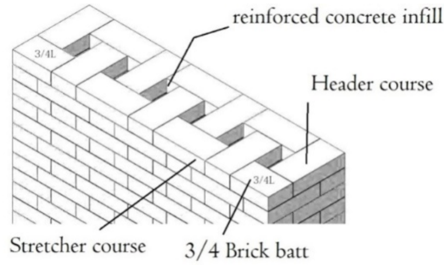

Fig. 2-Head-straight texture order of brick wall.

As it is obvious this kind of bearing walls in addition to having beautiful feature in both sides, demonstrates appropriate fastening and interlocking among the masonry units. In process of construction using this technique because of special arrangement of bricks, some regular interval voids appear all at the height of the wall. For reinforcement of this kind of walls these voids can be filled by high performance fiber concrete. Motivating above mentioned reasons, this type of URM construction were introduced and four specimens were constructed and tested under permanent vertical and cyclic horizontal loads. The mentioned voids in two of the specimen were filled using fiber concrete and for the others they remained unfilled. Experimental results were obtained, including failure modes, force-displacement hysteresis curves, shear behavior and envelope curves of force-displacement diagrams. Through experimental data analysis, a monographic investigation was performed to characterize seismic performance of mentioned walls, such as energy dissipation, ductility and stiffness degradation.

2. Test plan

2.1 Test specimens

In this research specimens were classified into two categories denoted by URM for the walls were laid up by Head-straight order (double Flemish texture) without in-filled fiber concrete cores and CRM for Head-straight order with inner fiber concrete cores. For each of mentioned categories two analogous specimens were built with the same masonry cohesion pattern and construction details. Out of four homological masonry walls, two of them were filled utilizing fiber concrete, after one week of curing. For performing a foundation, all specimens were placed on a mold with certain dimensions including a prefabricated mesh rebar. The foundation concrete was placed until the second layer of the wall from the bottom. Ultimately loading concrete beam (with two holes to install loading utilities) was mounted on the top of the wall. It worth noting that aspect ratio (H/L) for all specimens was considered 1 because of square shape of all masonry specimens.

2.2 Material properties

Prior to carrying out the cyclic test on masonry panels, mechanical properties of constituent material namely bricks, mortar and fiber concrete through a set of multiple tests were obtained.

2.2.1 Brick, mortar and fiber concrete

With regard to the mortar, composition of component materials according to ASTM C 144 - 11 [10] is reported in **Table 1**. The amount of water was decided to produce suitable workability. In case of fiber concrete, component materials were mixed together by gradually adding the amount of water until the achievement of optimum consistency. Thereafter steel fibers with the length of 35 mm (see Fig. 5) were gradually added to the concrete to avoid bunching in the mix. The yield and ultimate stress of the fibers were respectively 600 and 900 MPa.

Considering quality and high strength of Japanese bricks (having compressive strength of about 50 *MPa*) and regarding to the quality of brick units in Middle East countries we preferred to import medium strength units from china. The bricks employed were solid baked clay bricks by average size of 50×110×240 mm^3. All bricks were entirely saturated before construction. In order to define mechanical properties of the bricks in line with ASTM C 67 - 12 [11], uniaxial compression tests on four specimens of 50×110×110 mm^3 size, obtained by cutting common bricks were performed. Tests were conducted in line with ASTM C 109 / C109M – 12, ASTM C78 / C78M – 10, ASTM C140 – 12a, ASTM C469 / C469M – 10 [12-15] in order to determine compressive and tensile strength, module of elasticity and Poisson ratio of component materials. For exploring the tensile strength of fiber concrete as required by ASTM C 1609/C 1609M – 05 [16] three prismatic specimens of 100×100×400 mm3 were produced and after 28 days of curing, were subjected to bending tests on three points. In **Table 2** average values of above mention experiments for all types of masonry elements are reported.

Table 1-Mortar and fiber concrete composition materials.

	Cement (kg/m3)	Water (kg/m3)	W/C	Lime (kg/m3)	Sand (kg/m3)	Grave (kg/m3)	Steel fiber (% of cement weigth)	Super plastisizer (kg/m3)
Mortar	208	325	1.56	237	1025	-	-	-
Fiber concrete	270	177	0.66	-	935	900	51.5%	2.7

Table 2-Mechanical properties of masonry components.

	$\sigma_{c\ (MPa)}$	$\sigma_{f\ (MPa)}$	$E_{\ (GPa)}$	υ	Density (kg/m^3)
Brick	8.02	0.73	9.2	0.15	1709
Mortar	10.6	0.75	28.7	0.2	1760
Fiber concrete	27	4.7	12.3	0.17	2380

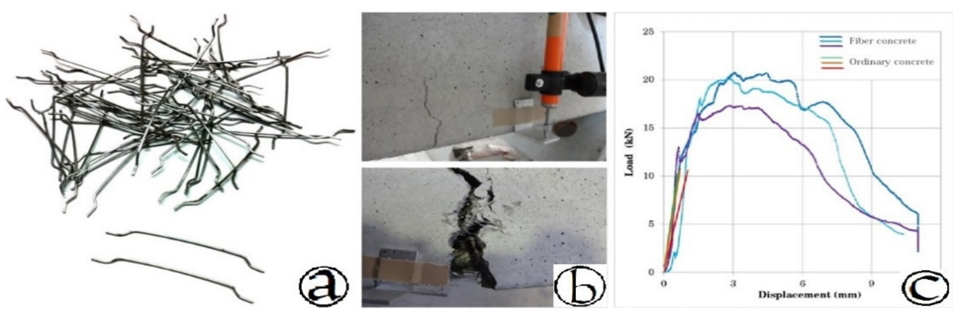

Fig. 3-a: steel fibers with double end hook, b: rupture test on fiber concrete prisms, c: load displacement diagram in rupture test.

2.2.2 Compressive strength of masonry

Masonry compressive strength was tested on three stack bonded prisms of five bricks each, under axial compressive loading. The main purpose was to determine mechanical characteristics of combined brick-mortar prisms and compare them with recommended value of relative standards. All prisms were performed in accordance to the code LUM B1, RILEM, 1994b [17]. The joints were kept uniform thickness of about 15 *mm* and filled with mortar. Each specimen was tested after curing of 40 days, which was a sufficient time for hardening of the lime mortar. **Fig. 4** and **Table 3** present the specimen test setup, failure mechanism and the obtained mechanical properties of masonry. The modulus of elasticity in compression was approximately 945, which was slightly (5%) less than the recommended value in EN 1996 Eurocode 6 [18].

Fig. 4-Compression test on masonry prisms.

Table 3-Compressive strength of masonry prisms.

Sample	Max Load (kN)	Compressive strength f (kg/cm^2)	Modulus of elasticity E(kg/cm^2)	Ratio E/f
1	9064.1	34.3	30725	895
2	8289.9	31.4	31421	1001
3	8102.6	30.7	28811	940
	Mean *f*	32.1	30364	945
	f_k=f/1.2	26.8		

3. Cyclic test on masonry panels

During cyclic test, masonry panels are subjected to reversal in-plane lateral loads such as those induced by seismic actions. In this kind of test, masonry are subjected to constant vertical forces representative of gravity dead and live load in line with horizontal cyclic displacement applied on the top of the wall. **Fig. 7** illustrates displacement history that was applied during the test. It is known that the behavior of masonry walls when subjected to in-plane cyclic loading test is severely affected by applied vertical load [6]. Therefore in this study, tests were performed under two different levels of vertical loads. From the inspected prototype in brick masonry building one up to three stories, values for vertical stresses close to 1-2 kg/cm^2. Therefore to provide results due to general validity two vertical load levels with magnitudes of 1 and 2 kg/cm^2 were considered.

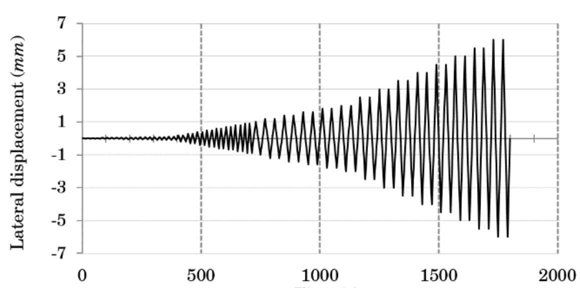

Fig. 7-Cyclic displacement time-history.

3.1 Test setup and instrumentation

Test setup regarding to perform cyclic test is illustrated on **Fig. 8.** Load application was manually controlled by hydraulic actuators with load capacity of 400 kN in horizontal direction and 3000 kN in vertical direction. The magnitude of vertical stress on the panel was kept constant during the test. Necessary vertical load intensity was manually tuned to the required level by use of screw-operated jack. Thereafter horizontal displacement until reaching the target displacement were imposed to the specimen in one direction and then in the opposite direction for two cycles. Details of dimension and arrangement of main LVDTs in the tests to measure displacements is illustrated in **Fig. 9** and were recorded automatically by a computer and data acquisition system. A large amount of experimental data was acquired during the test and the appearance and propagation of cracks were carefully observed by eye. The most important results are summarized and presented through the obtained failure modes, force-displacement hysteresis curves, envelope of force-displacement hysteresis curves, stiffness degradation of the walls at repeated cycles and energy dissipation capacity.

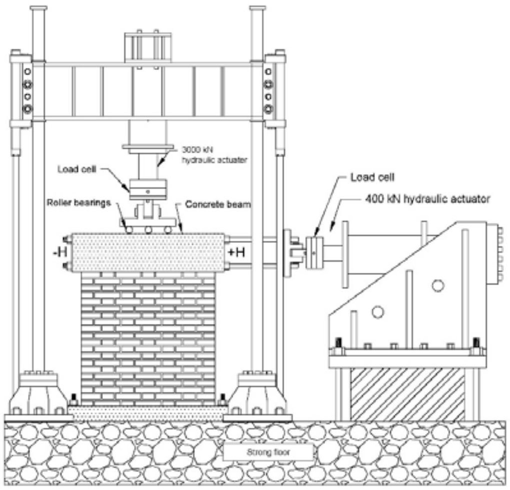

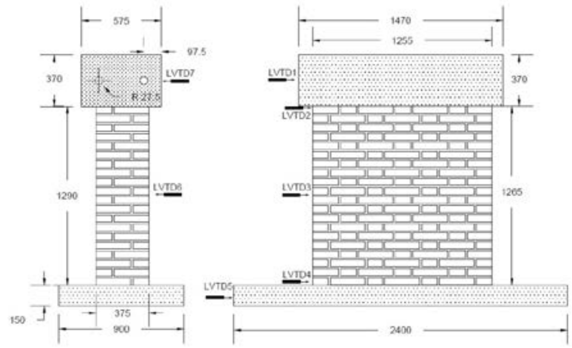

Fig. 8-Test setup system for cyclic test on panels. **Fig. 9-**Dimensions of specimens for cyclic test.

4. Test Results

4.1 Failure modes

Generally speaking, the walls exhibited flexural failure mode. In process of loading the flexural moment at the bottom of the panel accumulated as the load increased. Once the tensile stress associated with the flexural moment exceeded the tensile strength of the mortar, the first horizontal cracks appeared at the margin of the first or second from the bottom and tend to develop to the center of the panel. After the cracks on the sides of the specimens joined together in the center, all the walls started to demonstrate rocking behavior revolves around the center.

With present research, it was confirmed that behavior of internal concrete columns was highly integrated with the behavior of masonry components with aspect ratio less than 1.0. No bulged phenomenon was observed during the tests. For all the specimens no diagonal cracks were observed throughout the test and the failure of the walls caused by separation from the bottom. It was observed that the cracks on both front and back side developed synchronously, indicating symmetrical precision of construction and loading condition.

Fig. 10-Cracking pattern and failure modes of the specimens.

4.2 result of horizontal load and displacement

After performing load-displacement test on masonry walls a large amount of experimental data was acquired. The most important results are summarized and presented in **Table 5**, including P_{cr}, peak load P_u, failure load P_u and their corresponding displacements. According to rocking behavior of all specimens failure load was considered corresponding load on displacement of 3 mm. Based on the results, a significant improvement of shear capacity of CRM walls compared with URM walls was achieved. The maximum forces obtained in the core filled specimens were higher than the corresponding load obtained in the unreinforced specimens, varying within the range of 24 to 106%. Same effects were achieved in the other two limit states. Beside this in term of deformation capacity, the data revealed an interesting effect related to the crack limit (Δcr). The data presented **Table 5** revealed a higher amount of cracking limit of unreinforced walls loaded with vertical stress of 1.0 kg/cm^2 than that of the strengthened walls. Reverse consequence was achieved in conjunction with peak displacement (Δ_{peak}).As mentioned the deformation capacity in ultimate limit state of the all specimens was decided 3mm in order to rocking behavior.

Table 5-Specimen parameters and results of load-displacement.

Specimen	Length L[mm]	Height L[mm]	H/L	σo Vertical stress [kg/cm^2]	σo /fk	P_{cr}(kN)	Δ_{cr} (mm)	θ_{cr}%	P_{peak}(kN)	Δ_{peak} (mm)	Pu (kN)	Δ_u (mm)
URM 1	1255	1265	1	1	0.031	17.61	0.183	0.014	30.26	0.57	26.86	3.0
URM 2	1255	1265	1	2	0.063	19.93	0.193	0.015	35.06	0.60	47.79	3.0
CRM 1	1255	1265	1	1	0.031	21.09	0.133	0.010	45.12	0.81	52.80	3.0
CRM 2	1255	1265	1	2	0.063	31.18	0.150	0.012	72.56	1.20	79.95	3.0

4.3 Hysteresis diagrams and envelope curves

Hysteresis diagrams as well as envelope curves can trace the development of horizontal displacement on top of the wall during the cyclic loads. The hysteresis diagrams and envelope curves are shown in **Fig. 11** and **Fig. 12**. Envelope curves comprehensively reflect the shear capacity and seismic response of the wall. From the envelope curves and hysteresis diagrams, loading process of all the walls can be divided into three steps:

1-*Elastic phase*: this step starts from the beginning to the appearance of the first limit state. Hysteresis curves as well as envelope curves remained linear and the residual displacement of the specimens was small. Load was applied to the specimens in all stages under displacement control. At the end, cracks were appeared on the sides of the specimens on the margin of the bottom. The hysteresis loops is narrow and its area is negligible.

2-*Plastic phase*: This stage starts from cracking of the specimen to the peak load. As was expectable, rocking behavior was occurred for masonry walls after the load reached to a certain amount. Therefore corresponding load to 0.017% of lateral drift was defined as peak load for all the obtained results. There was an obvious increase in this stage on residual displacement as well as hysteresis loop area. In the first or second margin from the bottom horizontal cracks developed inward and tend to join up.

3-*Failure and rocking phase*: This stage starts from peak load (plastic stage) to the load corresponding to displacement 3 mm (Drift≈0.023 %). The peak value of the cyclic load for almost all specimens remained unchanged due to wobbling of the wall revolving around the center and the residual displacement was increased significantly. The area under the hysteresis loops increased sharply. Generally speaking the specimens demonstrate consistent reaction against horizontal lateral loads.

As is noticeable from **Fig. 11,** hysteresis loop of specimens CRM 1 and 2 covered a larger area than specimen URM 1and 2 indicating improved energy dissipation capacity for concrete filled masonry panels which signify the role of slim fiber concrete columns on absorbing the energy imposed to the structure. Similarly the same conclusion can be drawn from the comparison between the cyclic loops regarding to specimens CRM 1 and CRM 2 which indicate that the increase of vertical stress on cyclic test lead to raise of energy dissipation by the specimen. This performance was also detected in other studies as well [6,19,20].

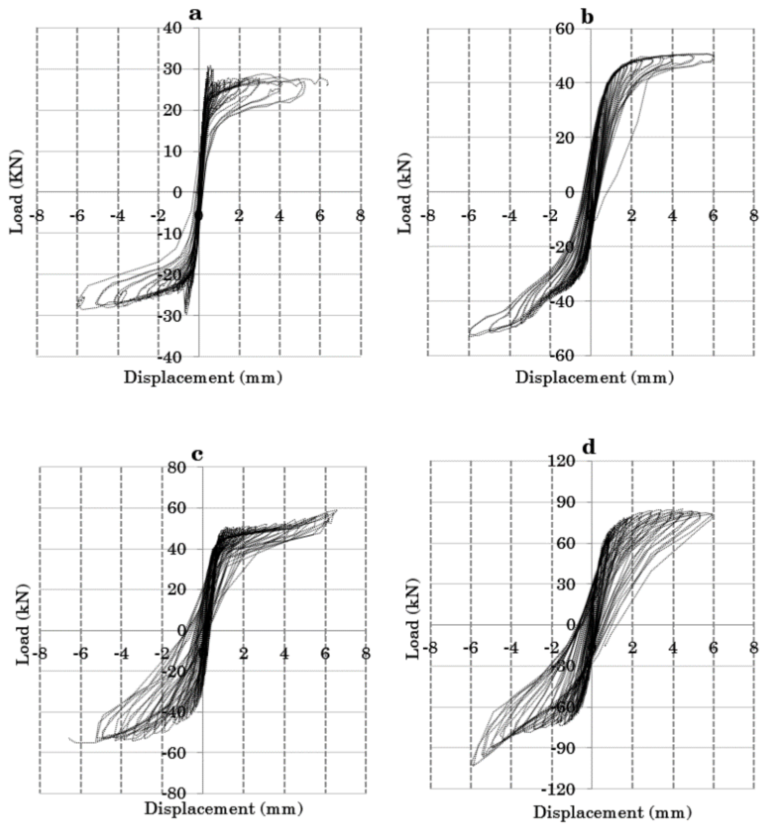

Fig. 11-Horizontal load-displacement diagrams (hysteresis curves), (a,b) respectively for URM 1,2 and (c,d) respectively for CRM 1,2.

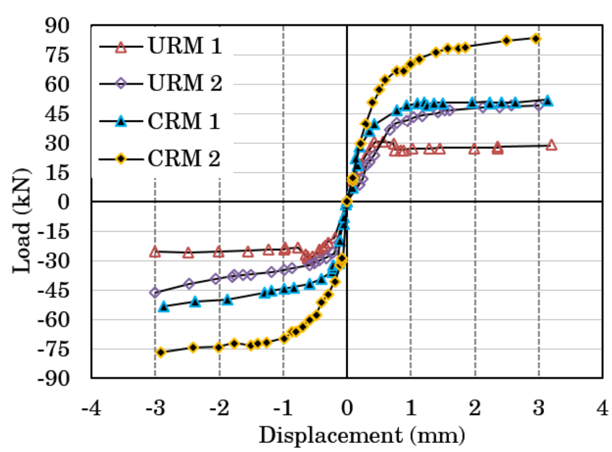

Fig. 12-Envelope curves of hysteresis diagrams.

4.4 Idealization of force-displacement diagrams

In order to simplify design and analysis of masonry walls, concept of idealized force-displacement curves is presented by taking into account the equal energy dissipation capacity of the actual and the idealized wall [6].

Bilinear idealization for load-displacement diagrams that is suggested by Tomazevic [21] was used in order to evaluate the in-plane seismic performance in terms of nonlinear deformability. For this, elastic shear stiffness k_e was defined by the slope of the secant passing through the origin and a point on the observed load-displacement envelope curve where the load equals 0.4 P_{peak} (As required by ASTM E 2126-02a [22]). Thereafter according to Eq.(4.4.1), maximum yield point (P_{yield}) of the idealized envelope was calculated considering the circumscribing an area equal to the area enclosed by observed load-displacement, between the origin, the ultimate displacement and the displacement axis.

$$P_{yield} = k_e \left(\Delta_u \sqrt{\Delta_u^{\,2} - 2\, {}^{A_{env}}\!/_{k_e}} \right) \qquad (4.4.1)$$

In which A_{env} is the area under the observed load-displacement envelope curve from zero to ultimate displacement.

Fig. 13 demonstrates a comparison of the results obtained from the bilinear idealization of the observed load-displacement envelops. As it can be seen from the graph despite strengthening significantly improves the lateral load resistance capacity of the walls, the deformation capacity of the walls was not proportionally increased in all the specimens. Also the strengthened panels loaded with higher level of vertical stress exhibited higher strength than the unreinforced one. This behavior can be described by the higher principal tensile stresses required to produce failure of the panel [jacketed].

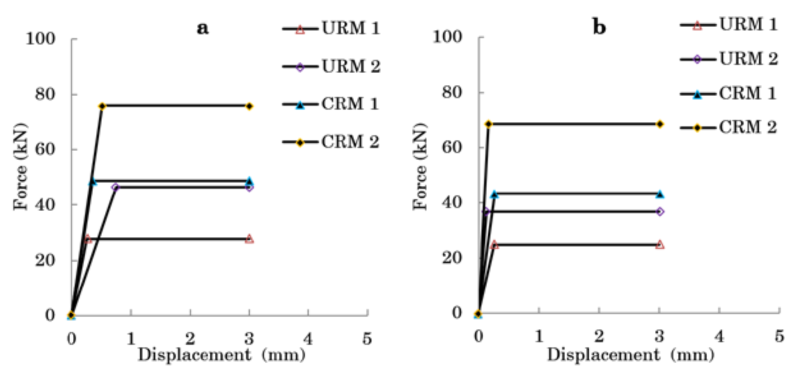

Fig. 13-Comparison of the idealized load-displacement diagrams. (a) Positive part of the curves (b) Negative part of the curves

4.5 Ductility and stiffness degradation

With the help of bilinear idealization ductility coefficient as the most common and essential index of structures subjected to cyclic loads was calculated by the means of equation (4.5.1).

$$\mu_u = \frac{\Delta_u}{\Delta_e} \qquad (4.5.1).$$

The bilinear idealization discovered interesting consequence related to the ultimate ductility factor (μ_u). The results presented in **Table. 6** revealed a higher ductility of URM and CRM walls loaded with the higher level of vertical load (2 kg/cm^2). The data show that, despite existing of concrete cores increased load capacity of the wall in all limit states however because of reduction of the displacement in mentioned states, no appreciable difference between the ductility of cored masonry walls in comparison with URM specimens pre-stressed with the same level of vertical load was observed. With regard to stiffness of the specimens, the secant stiffness ($K_{s,i}$) was calculated for each load cycles according to Eq. (4.5.2).

$$K_{s,i} = \frac{F_{max,i}}{\Delta_{max,i}} \qquad (4.5.2).$$

In which $K_{s,i}$ is the secant stiffness at the ith cycle, $F_{max,i}$ is the horizontal load at maximum displacement at ith cycle and $\Delta_{max,i}$ is maximum displacement at ith cycle. The results in three stages: K_e, K_{cr} and K_u (See **Table 6**) indicate a sharply increase between the stiffness coreless and core filled panels. The increase varies in the range of 62–101%, indicating that concrete cores have significant and effective role in the increase of the stiffness of the panels. In term of deformation capacity, CRM 2 was the first that started to crack, while URM 2 was the last. Quite different and inconsistent results on displacement at elastic limit were obtained. CRM 1 exhibited its maximum load capacity in crack limit at a very low level of displacement of 0.133 mm, while URM 2 reached its crack load capacity at a displacement of 0.193 mm. As mentioned before for all specimens the ultimate displacement because of rocking behavior was decided 3 mm.

Table 6-Results of stiffness and ductility factor

Specimen	P_{cr}	Δ_{cr}	P_{peak}	Δ_{peak}	P_u	Δ_u	P_e	Δ_e	K_{cr}	K_{peak}	K_u	K_e	μ_u
URM 1	17.61	0.18	30.26	0.57	26.87	3.0	26.36	0.26	96.23	53	8.95	99.81	11.35
URM 2	19.93	0.19	35.01	0.60	47.79	3.0	41.67	0.44	103.51	58.44	15.93	170.13	13.34
CRM 1	21.09	0.13	45.12	0.81	52.80	3.0	46.14	0.31	159.17	56.05	17.60	161.85	9.78
CRM 2	31.18	0.15	72.56	1.2	79.95	3.0	72.10	0.34	207.83	60.46	26.65	284.25	11.96

Fig. 14 demonstrates the development of stiffness degradation with increasing of displacement cycles in the test. All the walls demonstrate similar stiffness degradation with the increase of lateral displacement. This trend of degradation complies with a power function that is not remarkably different among the walls [21]. As it is obvious, the secant stiffness of the walls sharply decreased at the elastic limit, the degradation speed of the stiffness slow down significantly from the end of elastic stage to the plastic stage and then tend to be constant at the failure stage. It seems that vertical pre-compression level has much effectiveness on the decay of stiffness degradation slope, in case of cored panels.

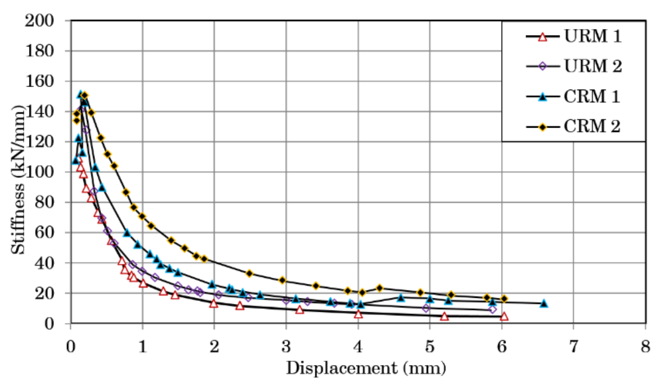

Fig. 14-Stiffness degradation curves referring to URM and CRM walls.

5. Conclusion

This paper presents a complete experimental protocol for core less and core filled Head-straight masonry walls. This experimental program was needed as this kind of construction has been used frequently in regions of high seismic risk and there were no previous experimental information available about its seismic performance of such structures. It contributes to an improved insight into the in-plane behavior of masonry walls considering the influence of pre-compression levels. From the experimental program summarized in this paper, the following observations can be made:

1- About failure category as was anticipated (because of high strength of masonry units and small amount of H/L ratio) rocking mechanism was observed in all test specimens. In case of URM 1 because of small amount of vertical stress, peak load was observed on hysteresis diagram as well as envelope curves.

2-experimental results proof that, existing concrete columns increased lateral resistance of the head-straight masonry panels in all limit states. This increase of lateral resistance in case of URM 1 and CRM 1 in crack limit was 20% and in ultimate limit was 97%. It is interesting to mention that despite the increase of the load in cracking limit, corresponding displacement was decreased up to about 30%. This can be due to the effect of the cores on the increasing of the stiffness of the walls. Also for URM 2 and CRM 2 the enhancement of lateral resistance in cracking and ultimate limit states was 56% and 107% which reveal that concrete cores will affect greater if the level of vertical stress increase.

3- Level of pre-compression load showed direct correlation with the lateral resistance of the walls. For URM 1,2 and CRM 1,2 the wall loaded to a higher pre-compression load, achieved higher lateral capacity in all limit states. The amount of this increase for URM walls for crack limit was 13% and for CRM walls was 48%. This kind of behavior also was observed in other studies as well [19,20]. This behavior can be explained by the higher principal tensile stresses needed to generate failure of the walls.

4-In conjunction with stiffness, all the panels demonstrate similar degradation process during the test. Secant stiffness of the masonry panels decreased sharply at elastic phase. The degradation speed slows down significantly from the end of the elastic phase to the plastic stage and tended to be constant at the failure phase. Coreless panels clearly exhibited lower initial stiffness than concrete cored ones, and a more rapid decrease in the first phase. Beside this, existing internal concrete cores demonstrated obviously positive effect on the development of the stiffness of the specimens in all stages. This increase in some cases was about 40%. Also in case of cored panels, it was found that the amount of vertical pre-stress value has much more impact on the enhancement of stiffness of the specimens.

In this context, further theoretical research will be conducted not only on the characterization of concrete cores but also on the description of the out-of-plane behavior under simulated seismic load. Hence, we can succeed to results that can provide accurate guidelines for design and implementation of this kind of masonry constructions.

ACKNOWLEDGEMENTS

Financial support for this testing that was provided by the Ministry of Education, Science and Technology of Japan(26303007-01) is acknowledged.

References

[1] P. Medeiros, G. Vasconcelos, P.B. Lourenço, J. Gouveia, (2013) Numerical modelling of non-confined and confined masonry walls. Construction and Building Materials 41 968-976.

[2] M. ElGawady, P. Lestuzzi, M. Badoux, A review of conventional seismic retrofitting techniques for URM. 13th International Brick and Block Masonry Conference Amsterdam, July 4-7, 2004.

[3] C. Calderini, S. Cattari, S. Lagomarsino, The use of the diagonal compression test to identify the shear mechanical parameters of masonry, Construction and Building Materials 24 5 (2010) 677-685.

[4] A. Gabor, E. Ferrier, E. Jacquelin, P. Hamelin, Analysis and modelling of the in-plane shear behavior of hollow brick masonry panels, Construction and Building Materials 20 (2006) 308-321.

[5] V.G. Haach, G. Vasconcelos, P.B. Lourenço, Parametrical study of masonry walls subjected to in-plane loading through numerical modeling. Engineering Structures 33 (2011) 1377-1389.

[6] S. churilov, E. Dumova-Jovanoska, In-plane shear behaviour of unreinforced and jacketed brick masonry walls. Soil Dynamics and Earthquake Engineering 50 (2013) 85-105.

[7] F. da Porto, G. Guidi, E. Garbin, C. Modena, In-Plane behavior of clay masonry walls: experimental testing and finite-element modeling, Journal of Structural Engineering 136 11 (2010) 1379-1392.

[8] X. Jianzhuang, P. Jie and H. Yongzhong, Experimental study on the seismic performance of new sandwich masonry walls Vol.12, No.1 earthquake engineering and engineering vibration March, 2013

[9] Deyuan Zhou, Zhen Lei, Jibing, In-plane behavior of seismically damaged masonry walls repaired with external BFRP Wang Composite Structures 102 (2013) 9–19.

[10] ASTM Committee C 144 -11, Standard specification for aggregate for masonry mortar, American Association State and Transportation Officials Standard 2011.

[11] ASTM Committee C 67 - 12, Standard test methods for sampling and testing brick and structural clay tile, American Association State and Transportation Officials Standard 2012.

[12] ASTM Committee C109/C109M-12, Standard test method for compressive strength of hydraulic cement mortars (using 2-in. or [50-mm] cube specimens), American Association State and Transportation Officials Standard 2012.

[13] ASTM Committee C78 / C78M-10e1, Standard Test Method for Flexural Strength of Concrete (Using Simple Beam with Third-Point Loading), American Association State and Transportation Officials Standard, 2010.

[14] ASTM Committee C140-12a, Standard Test Methods for Sampling and Testing Concrete Masonry Units and Related Units, American Association State and Transportation Officials Standard, 2012.

[15] ASTM Committee C469/C469M-10, Standard Test Method for Static Modulus of Elasticity and Poisson's Ratio of Concrete in Compression, American Association State and Transportation Officials Standard 2010.

[16] ASTM Committee C 1609/C 1609M – 05, Standard Test Method for Flexural Performance of Fiber-Reinforced Concrete (Using Beam With Third-*Point Loadin*g), American Association State and Transportation Officials Standard 2010.

[17] Rilem. Technical recommendations for the testing and use of constructions materials, LUM B1, Compressive strength of small walls and prisms, 1994 (b).

[18] Eurocode 6-Design of masonry structures Part1-1: General rules for reinforced and unreinforced masonry structures. EN1996-1-1:2005,CENBrussels; 2005.

[19] Haach VG. Development of a design method for reinforced masonry subjected to in-plane loading based on experimental and numerical analysis. PhD thesis. Universidade do Minho, Escola de Engenharia, Guimarães, Portugal; 2009.

[20] Tomaževič M, Weiss P. Robustness as a criterion for use of hollow clay masonry units in seismic zones: an attempt to propose the measure. Materials and structures, 1:1–19,2011. issn:1359-5997.

[21] Tomaževič M. Earthquake-resistant design of masonry buildings, series on innovation in structures and construction, vol.1. London: Imperial College Press; 1999.

[22] ASTM E Committee 2126-02a Standard Test Methods for Cyclic (Reversed) Load Test for Shear Resistance of Framed Walls for Buildings, American Association State and Transportation Officials Standard 2002.